UNIVERSITY OF CALIFORNIA,
IRVINE

# Spin torque driven magnetization dynamics in nanoscale magnetic tunnel junctions

DISSERTATION

submitted in partial satisfaction of the requirements
for the degree of

MASTER OF SCIENCE

in Physics

by

Chengcen Sha

Dissertation Committee:
Professor Ilya Krivorotov, Chair
Professor Zuzanna Siwy
Professor Wilson Ho

2016

# DEDICATION

To My parents, Zhenglian and Wenyu.

# TABLE OF CONTENTS

# LIST OF FIGURES

# ACKNOWLEDGMENTS

I would like to express my deepest appreciation to Professor Ilya Krivorotov. It is quite a privilege to work with him. I really learned a lot from his great knowledge of physics and sharp insights into problem solving. Without his guidance and help this dissertation would not be possible. I would also like to thank my committee members, Professor Zuzanna Siwy and Professor Wilson Ho.

I would also like to thank all my lab mates : Zheng Duan, Igor Barsukov, Brian Youngblood, Yu-Jin Chen, Andrew Smith, Han Kyu Lee, Jenru Chen, Jieyi Zhang, Alejandro Jara, Chris Safranski and Josh Dill. I have been received a great amount of help since the first day I joined the lab.

# ABSTRACT OF THE DISSERTATION


Spin torque driven magnetization dynamics in nanoscale magnetic tunnel junctions

By

Chengcen Sha

Master of Science in Physics

University of California, Irvine, 2016

Professor Ilya Krivorotov, Chair



This master thesis demonstrates our investigation on spin torque driven magnetization dynamics in nanoscale magnetic tunnel junctions. We develop field-modulation spin-torque ferromagnetic resonance to characterize magnetic anisotropy and magnetic damping in nanomagnets. Then we demonstrate a single-shot electrical technique to capture the magnetic dynamics during the spin-torque-induced switching. By improving the sensitivity, we can directly observe real-time oscillation before switching. Lastly, we focus on measurement of switching probability of magnetic tunnel junctions by applying electric pulses. We observe anomalous write error rate behavior in our magnetic tunnel junctions samples. Possible origins of this anomalous write error rate has been discussed.

# Chapter 1

# Introduction

Spin transfer torque is generated by the transfer of angular momentum from spin polarized electrons to a ferromagnet. This spin transfer torque provides an efficient way to manipulate the dynamic motion of the magnetization of a nanomagnet, and can be strong enough to induce magnetization switching and steady-state precession. This field of study draws enormous attention not only because spin transfer torque is essential in understanding fundamental physical phenomena, but also it makes the building block for future applications such as spin torque oscillators, magnetic random access memory.We have developed several new techniques to characterize such dynamics in nanoscale magnetic tunnel junctions.

In chapter 2, we will first discuss necessary background knowledge in this field. In chapter 3, we develop a new reliable methods to characterize material parameters such as magnetic anisotropy and Gilbert damping using spin-torque ferromagnetic magnetic resonance with field-modulation. By performing micromagnetic simulations, we can also determine other spatial-dependent parameters.

In chapter 4, we demonstrate a single-shot electrical technique to capture the magnetic dynamics during the spin torque switching of a magnetic tunnel junction in real time. With improved sensitivity, we can directly observe real-time oscillation before switching.

In chapter 5, we focus on measurement of switching probability of magnetic tunnel junctions by applying electric pulses. We observe anomalous write error rate behavior in our magnetic tunnel junctions samples. Possible origins of this anomalous write error rate has been discussed.

# Chapter 2

# Background

## 2.1 Spintronics

## 2.2 Tunnel Magnetoresistance

The Tunnel Magnetoresistance effect[10] refers to the change of resistance of a ferromagnetic/non-magnetic barrier/ferromagnetic metallic multilayer structure as the relative orientation of the magnetizations of two ferromagnetic layers changes. When the two layers have parallel magnetizations, the resistance is lowest and the resistance is maximum when magnetizations of two ferromagnetic layers are anti-parallel. Nowadays, the resistance difference between the maximum and minimum values can be as much as 100 per cent.

We first consider a simple case when electrons are passing through a single ferromagnetic layer. For a 3d transitional ferromagnetic layer like Ni, Co and Fe, ferromagnetism is coming from the exchange coupling of 3d electrons. In a simplified band structure for ferromagnetic metals, the exchange coupling results in an split of energy band for 3d electrons. As a result when the spin-up band and spin-down band are filled up to the Fermi level, there will be more spin-up electrons than spin-down electrons, which induces a net magnetization. On the other hand, the majority and minority spin bands also have different density of states at the Fermi level. The conduction properties of a metal are primarily determined by the electrons near the Fermi level. When spin unpolarized electrons consisting of equal numbers of spin-up and spin-down electrons travel in a ferromagnet, different spins experiences different resistances. Besides, different types of spins also experience different scattering at the interface due to the band structure mismatch. Overall, one type of spins has higher probability to transmit through than the other type.

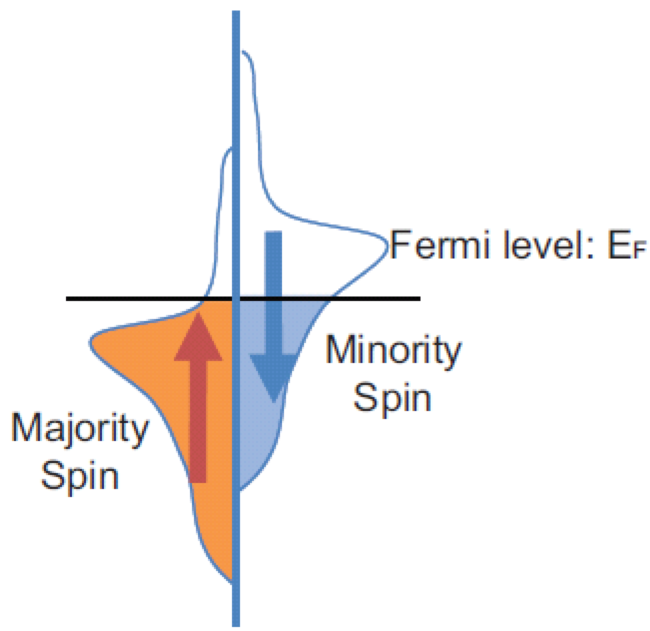


Figure 2.1: Band structure for ferromagnet. Due to energy split, the majority and minority spin bands have different of states at the Fermi level.

Now, we have two magnetic layers separated by a tunnel barrier. As it has been proposed by Julliere in 1975, the tunneling probability across the tunnel barrier,which can be treated as conductance in this case, is proportional to the density of states of both initial and final states. Then we have

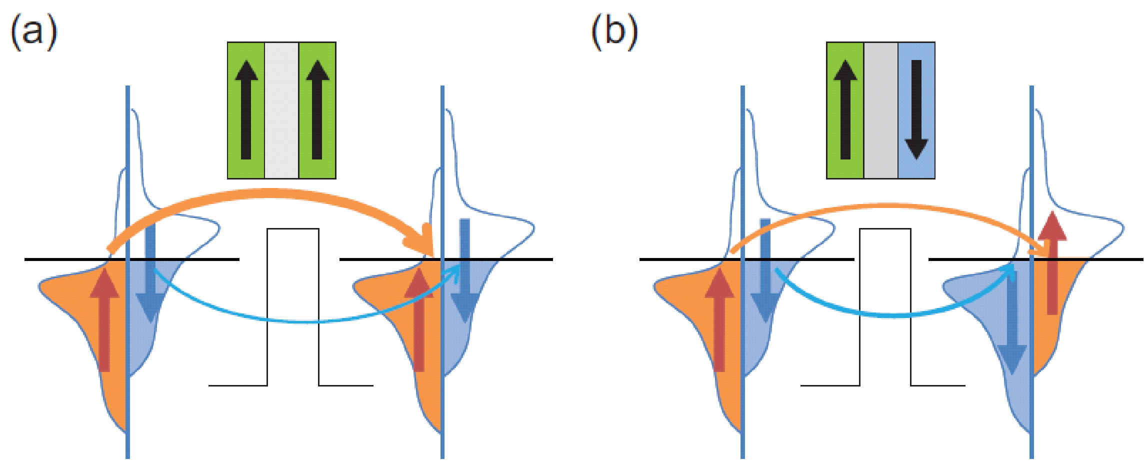


Figure 2.2: Illustration of tunnel magnetoresistance effect. (a)Configuration of two layers are parallel.(b)Configurations of two layers are anti-parallel.

$$\begin{aligned} G_p &\propto \rho_{L\uparrow}\rho_{R\uparrow} + \rho_{L\downarrow}\rho_{R\downarrow} \\ G_{Ap} &\propto \rho_{L\uparrow}\rho_{R\downarrow} + \rho_{L\downarrow}\rho_{R\uparrow} \end{aligned} \tag{2.1}$$

where $G_P(G_{AP})$ is the parallel(anti-parallel) conductance, $\rho_{L\uparrow}$ and$\rho_{L\downarrow}$($\rho_{R\uparrow}$ and$\rho_{R\downarrow}$) are densities of states for up and down spins of the left(right) ferromagnet. By definition, the spin polarization P is

$$P = \frac{\rho_\uparrow - \rho_\downarrow}{\rho_\uparrow + \rho_\downarrow} \tag{2.2}$$

Therefore the tunnel magnetoresistance ratio can be calculated as

$$TMR = \frac{R_{AP} - R_P}{R_P} = \frac{G_P - G_{AP}}{G_{AP}} = \frac{2P_L P_R}{1 - P_L P_R} \tag{2.3}$$

In early studies of MTJs,a TMR ratio of a few 10's of percent was achieved with amorphous aluminum oxide(AlO)barries. Most recently, single crystalline magnesium oxide(MgO) barries were predicted to provide a much higher TMR ratio due to the wavefunction match between the ferromagnetic electrodes and the tunnel barrier. TMR ratios of around 200 percent were then demonstrated and led to intensive studies in MgO bases MTJs mainly because of the high TMR ratio founded in this family[2].

## 2.3 Spin transfer torque

Spin transfer torque refers to the torque between electrons and local magnetization. As it is shown in 2.3, the direction of incident electron is randomly distributed in all directions. When electrons are entering a ferromagnetic layer, due to the fixed magnetization of this FM layer, electrons are parallel to the local magnetization will have high probability of transmission and on the other hand, the electrons having opposite direction will mostly be reflected. As a result, transmitted electrons will be aligned to the local magnetization and reflected. In this process, the angular momentum of incident electrons has been changed by local magnetization. On the other hand, the local magnetization also experience torque from incident electrons as well. This torque is called the spin transfer torque[19] [1] and can provide an efficient way to manipulate local magnetization as we shall see next.

Magnetic tunnel junction is the main device we have been studied. The device has a a structure of two ferromagnetic layers separated by a spacer. The mulitilayers are patterned into a elliptically-shaped nanopillar withe size normally around 60nm. The top and bottom of the devices are connected to electrical leads to allow current to pass perpendicularly through the multilayers.

The dynamics of the magnetization in the presence of spin transfer torque can be described

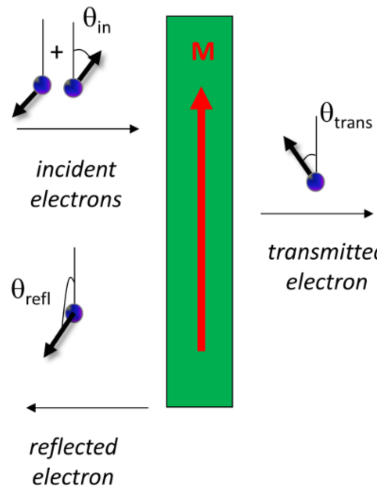


Figure 2.3: Schematic of electrons transmitting through and getting reflected from ferromagnet metal, with the transverse spin component absorbed during the process.

by the classical Landau-Lifshitz-Gilbert(LLG) equation including an additional term for the spin torque:

$$\frac{dM}{dt} = \gamma M \times H_{eff} + \alpha M \times \frac{dM}{dt} + g(\theta)\frac{\gamma \hbar I}{eV_{free}M_s} M \times (M \times M_{fix}) \tag{2.4}$$

where $H_{eff}$ is the total effective field including the applied field $H_{applied}$ and the anisotropy field $H_{ani}$ and $\alpha$ is the damping constant. The first term is the field torque term which makes the magnetization precess around the effective field direction. The second term is the damping torque which relates the energy dissipation. On average it points towards the equilibrium position of the magnetization, so that without any external excitation the magnetization will relax back to the equilibrium. The third term is the spin transfer torque. The direction of this torque depends on the direction of the electron flow. For electron flow from the fixed layer to the free layer, this torque is in the same direction as the damping torque assuming the fixed layer also along the effective field direction, in this case spin transfer torque works as additional damping torque. On the other hand, for electron flow from the free layer to the fixed layer, this torque works against the damping torque and thus can reduce the relaxation.

The first case we discussed is of less interest. For the second case we have the competition between spin transfer torque and damping torque[28]. Usually the spin transfer torque is small compared to the field torque. So the effect of spin transfer torque can be viewed as either increasing or decreasing the amplitude of the magnetic precession. In general, the magnetic dynamics excited by spin transfer torque can be categorized in to two types: switching and persistent precession.

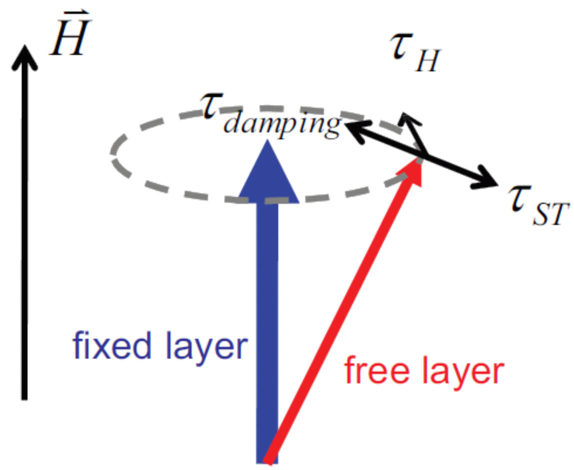


Figure 2.4: Direction of torques presented in the system.

## 2.4 Magnetic Switching

At zero or small field, both direction along the easy axis correspond to local energy minimums so it is possible to switch the magnetization between these two directions with spin transfer torque. For example, for a device with both free and fixed layers keeping at the easy axis direction and parallel to each other, if we flow a positive current defined as current flow from free to fixed layer, according to previous analysis, the spin transfer torque acts on the free layer is pointing away from the fixed layer and destabilizes this configuration so that the magnetic moment of the free layer goes into a precession around the easy axis. If we keep increasing the current, the amplitude of the free layer precession increases until it reaches the energy barrier which is around 90 degree. After the free layer changes direction, now the spin transfer torque will act as damping torque again and stabilize the magnetization. Similarly, if the magnetic tunnel junction starts in the anti-parallel configuration, a strong enough negative current can switch the free layer back to the parallel configuration. If we monitor the resistance of the device, it will exhibit a hysteresis loop as we sweep the current, as shown in the example

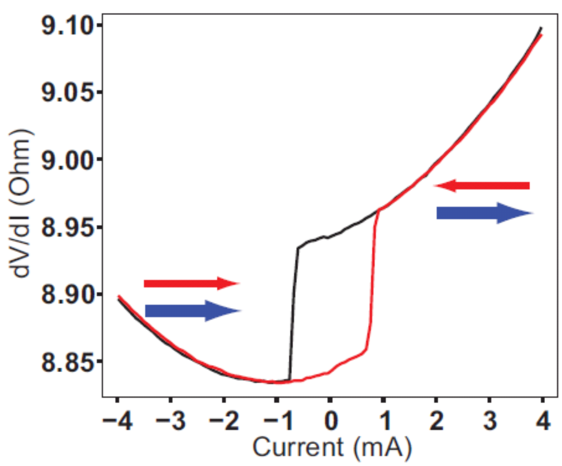


Figure 2.5: Differential resistance with respect to dc current. Arrows indicate magnetic state to be either parallel and anti-parallel.

The critical switching current $I_c$ is defined as the current required to achieve switching at zero temperature(no thermal excitations) . Above $I_c$, the spin torque is stronger than the damping torque and drives the free layer moment to switch direction.[Fig] illustrate the switching process. The switching proceeds via a precessional motion of the magnetization with increasing amplitude[9]. The switching time is defined as the following :

$$t_s \propto \frac{1}{I - I_c} \tag{2.5}$$

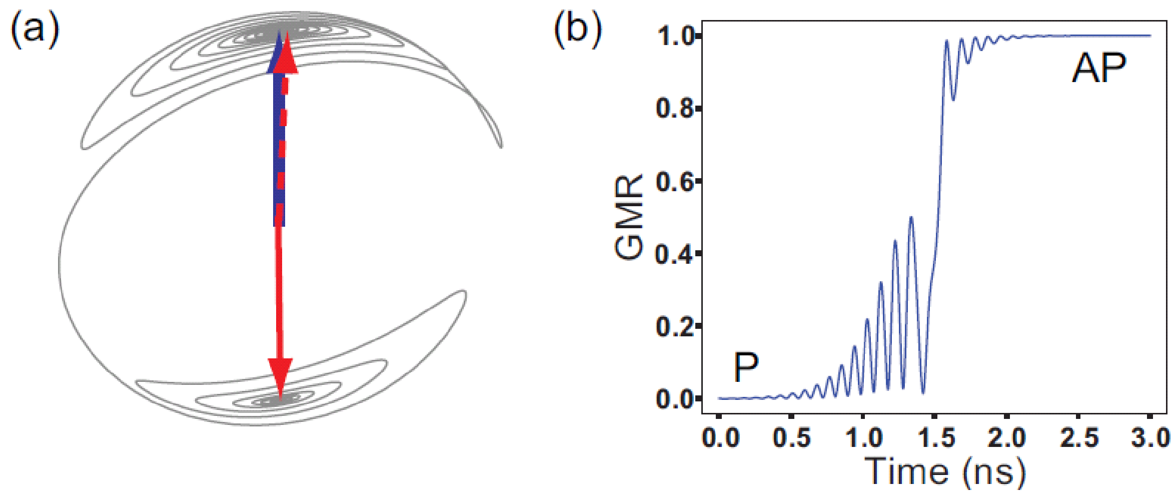


Figure 2.6: An example of a simulated spin transfer switching event.(a)Switching trajectory. Dotted lines show initial state of free layer. Solid line shows the switching (b) Normalized resistance value as a function of time

Now if the applied current is smaller than the critical current, the spin torque is not strong enough to drive the free layer moment to directly overcome the energy barrier to achieve switching but only to excite magnetic precession at small amplitudes. At finite temperatures, switching can still occur due to thermal excitations. This thermal-assisted magnetization reversal can be described by the Neel-Brown relaxation time:

$$P(t) = 1 - exp(-t/\tau) \tag{2.6}$$

where t is the observation time, and $\tau$ is the relaxation time which is given by

$$\tau = \frac{1}{f_0} \exp E_b/k_B T \tag{2.7}$$

Here $f_0$ is the attempt frequency, $E_b$ is the energy barrier and T is the temperature. Thermal assisted switching can be modeled by a fluctuating field with a Gaussian stochastic process. The relaxation time $\tau$ can be modified as the following:

$$\tau = \frac{1}{f_0} \exp[\frac{E_b}{k_B T}(1 - \frac{I}{I_c})] \tag{2.8}$$

## 2.5 Spin-torque Ferromagnetic Resonance

As we mentioned above, when the spin transfer torque is small, the magnetization will not reverse however experience a persistent precession. By applying AC current, excited magnetic precession can be detected by measuring a mixing DC voltage from the product of the resistance oscillation and the ac current. This Spin-transfer Ferromagnetic Resonance (ST-FMR) [21][26] is similar to the traditional ferromagnetic resonance, but can be performed in much smaller devices. The ST-FMR technique can be used to characterize important material properties such as voltage-controlled-anisotropy[13][33][30], magnetic damping[17], field-like torque[22] along with the spectrum of magnetic excitations of the MTJ[8][16], which is not important for understanding basis physic phenomena like spin-tunnel process but also essential for characterizing and optimizing the MTJs for future applications. In Chapter 3, I will describe an improved technique to measure Spin-torque Ferromagnetic Resonance with field modulations.

# Chapter 3

# Field-Modulated Spin-torque Ferromagnetic Resonance

## 3.1 Spin-torque Ferromagnetic Resonance

Ferromagnetic resonance (FMR) is the main technique to study dynamical properties of magnetic materials. However, conventional FMR detection methods lack the sensitivity to measure individual sub-100-nm-scale devices that are of interest for fundamental physics studies and for a broad range of memory and signal-processing applications[21]. Sankey and Tulapurkar et al. demonstrated that they can excite precession not by applying an ac magnetic field as is done in other forms of FMR, but by using the ac spin-transfer torque from a spin-polarized ac current.When an alternating current is applied to the sample[21][26], spin transfer torque induces magnetization dynamics, leading to a changing sample resistance from the sample magnetoresistance. Alternating current and resistance get mixed and give rise to a direct voltage, which can be measured using lock-in technique. By sweeping the frequency of the applied alternating current, a peak in the direct voltage generated by the sample can be observed when the applied frequency matches the resonance frequency of the sample. This technique is called spin-torque ferromagnetic resonance[21] and has been widely used to understand magnetization dynamics induced by spin transfer torque. Analysis of the resonance frequencies, amplitudes, linewidths, and line shapes as a function of microwave power, dc current, and magnetic field provide detailed new information about the exchange, damping[12][6], and spin transfer torques that govern the dynamics in magnetic nanostructures[21].

When the spin polarized current is applied near the resonance frequency, it can drive the precession of magnetization by effectively pushing and pulling the magnetization (depending on the instantaneous polarity of the RF current) in phase with its natural precession. In the case of MTJs, the fixed layer acts as a spin filter which polarizes the current passing through the free layer in the direction of the fixed layers magnetization. In this discussion, it is assumed that the fixed layer magnetization is ideal and completely locked in place. This oscillation of the free layer magnetization will also produce an oscillation of the device resistance due to the varying relative angle between fixed and free layer magnetizations. The time-dependent resistance can be expressed as the expansion [21]:

$$R(t) = R_0 + \Delta R(t) = R_0 + Re(\sum_n \Delta R_{nf} e^{in\pi ft}) \tag{3.1}$$

When the $\Delta R_{nf}$ can be can be complex. Since the fixed layer is supposed to be stationary, the resistance thus oscillates as the magnetization of the free layer m,which is the solution of the LLGS equation. The mixing voltage signal being measured can be composed of rather complex form, however, it is possible to write the voltage as

$$eq : FMRV_{mix} = V_s S(\omega) + V_a A(\omega) \tag{3.2}$$

Where $\omega$ is the driven frequency and $V_s$ and $V_a$ are functions of the spin-torque vector and other magnetic parameters. In this case, the fitting can be simplified as only four fitting parameters. In order to study magnetic information such as anisotropy field and Gilbert damping parameter, one can measure the spectrum and fit fro resonance frequency and linewidth as a function of applied field. The theoretical model used here is given by the Kittel equation[11].

$$f_{res} = \gamma(H_k \pm |H_{dip}| + H_{ext}) \tag{3.3}$$

Here $f_{res}$ is the resonance frequency extracted from fitting the curve. $H_{dip}$ is the center of hysteresis loop and $H_{ext}$ is the external magnetic field. The Gilbert damping parameter, given the easy axis approximation, is

$$\alpha = \frac{\Delta f_{res}}{f_{res}} \tag{3.4}$$

It should be noticed that in this equation3.4, the linewidth $\Delta f_{res}$ is the half-width-at-half-maximum(HWHM).

## 3.2 Experimental Technique

However, this rectified ST-FMR methods suffers from frequency-dependent non-magnetic background signals due to non-linearities and impedance mismatches within the microwave circuit. For example, measurements of MTJ with collinear free and pinned layer magnetizations (the STT-MRAM geometry) are challenging with the rectification ST-FMR because magnetic signals are typically weak. Fig.3.2(a) shows a typical spectrum measured by conventional ST-FMR with amplitude modulations. Despite the excitations of several spin wave modes, the spectrum has changing background and lots of standing wave from the circuit, thus it would be very hard to quantitatively fit to extract resonance frequency and linewidth. The other two main methods of spin-torque ferromagnetic resonance measurement, time domain[27] and network analyzer[32] require non-zero bias therefore fail to allow studies of MTJ magneto-dynamics at zero bias

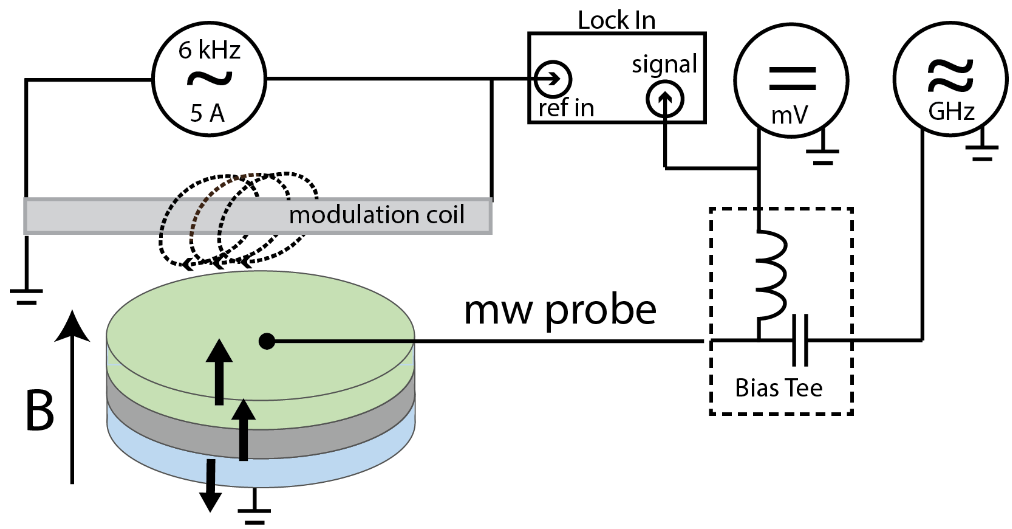


Figure 3.1: Sketch of our field-modulation set-up.

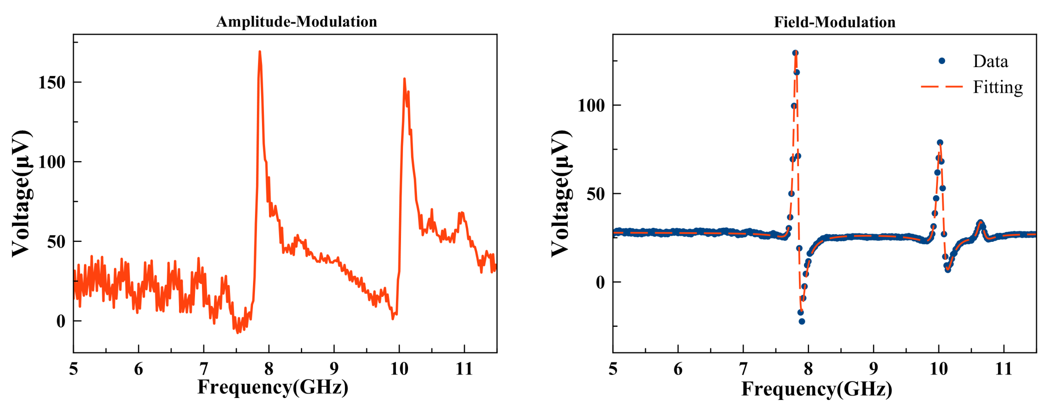


Figure 3.2: (a)Typical ST-FMR spectrum taken with conventional amplitude modulation.(b)ST-FMR spectrum taken with field modulation at the same sample.

To solve this problem, We make ST-FMR measurement with field modulation technique[7]. A modulation coil is placed just above the sample as shown in Fig.3.1. We then apply kHz-range sinusodal current of a few Amperes in the coil and generate a few Oersteds alternating magnetic field. The modulation field from the coil is perpendicular to the nanopillar. A continuous microwave current is applied to the sample via a bias tee, and a rectified voltage generated by the sample is measured by a lock-in amplifier at the field modulation frequency. In this case, by sweeping the driving frequency, any non-magnetic background noise would be eliminated. Fig.3.2(b) shows a typical field-modulation spectrum taken at the same sample comparing with Fig.3.2(a). Now we have a much better flat baseline and the standing wave is greatly reduced from the signal.

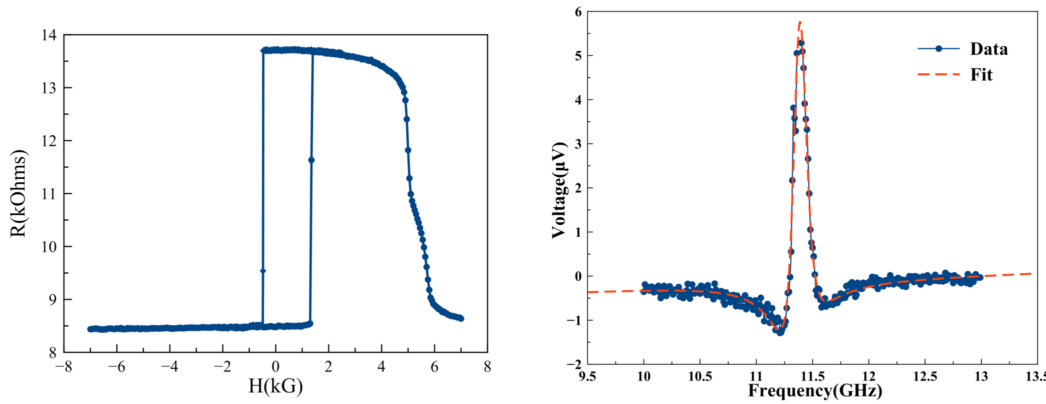


Figure 3.3: (a)Magneto-resistance plot of the sample studied. SAFTop layer start to flop around 4.5kG. (b)Blue dot:Typical ST-FMR spectrum with only lowest-frequency mode. Red dash line: Fitted curve to extract resonance frequency and linewidth.

The MTJ nanopillar we have measured has a lateral size of 65*30nm with a stadium shape: approximately half-circular on both ends of a rectangular. The main functional layers structure of our sample are SAFBottom(1.67)/SAF spacer(0.41)/SAFTop(1.1)MgO(0.8)FreeLayer(2.4) multilayer(thickness in nm). Fig.3.3(a) shows the magneto-resistance plot with magnetic field applied perpendicular to the sample. Around 4.5kG, the resistance of the MTJ start to decrease and eventually switch back to low-resistance parallel state. This is due to the flopping of SAFTop layer. We identify 4.5kG to be the breakdown field and will use it for later discussion.Fig.3.3(b) shows the ST-FMR spectrum focusing on the lowest-frequency mode. We are now going to derive the mathematical equation to extract resonance frequency and linewidth from the curve.

## 3.3 Gilbert Damping Evaluation

As we discussed in the previous chapter, the line shape $V_{mix}(f)$ without field modulation is a sum of symmetric $S(f)$ and antisymmetric $A(f)$ Lorentzians $V_{mix}(f) = V_s S(f) + V_a A(f)$, where $S(f) = \frac{1}{1+(f-f_r)^2/\sigma_r^2}$, $A(f) = \frac{(f-f_r)/\sigma_r}{1+(f-f_r)^2/\sigma_r^2}$, $f_r$ is the resonance frequency and $\sigma_r$ is the linewidth. When the modulation field is small, the RMS voltage signal $\tilde{V}_{mix}(f)$ measured by the lock-in amplifier is proportional to the first derivative of the rectified voltage $V_{mix}(f)$ with respect to the modulated variable-the external magnetic field $B$.

$$\begin{aligned}\tilde{V}_{mix}(f) =& B_m \frac{dV_{mix}(f)}{dB} = B_m[\frac{dV_s}{dB}S(f) + \frac{dV_s}{dB}A(f) \\ &+ \frac{1}{\sigma_r}\frac{d\sigma_r}{dB} \times (2V_s A^2(f) + V_a[2A^3(f)/S(f) - A(f)]) \\ &+ \frac{1}{\sigma_r}\frac{df_r}{dB}(2V_s S(f)A(f) + V_a[A^2(f) - S^2(f)])]\end{aligned} \tag{3.5}$$

Here $B_m$ is the RMS amplitude of the modulation field, and the last term proportional to $df_r/dB$ is usually dominant. If $V_s$ and $V_a$ are weak functions of magnetic field then the symmetric part of $\tilde{V}_{mix}(f)$ is proportional to $V_a$ and the anti symmetric part is proportional to $V_f$.

Fig.3.4(a) shows the fitted resonance frequency of the quasi-uniform modes respect to the external magnetic field. As we expect from Kittel equation, there is a good linear relation. Making an easy axis approximation, the Kittle equation is

$$f = \gamma(H_k \pm |H_{dip}| + H_{ext}) \tag{3.6}$$

Here $H_{dip}$ is the center of hysteresis loop and $H_{ext}$ is the external magnetic field. The quasi-uniform mode frequency at zero field gives magnetic anisotropy field of the free layer ($H_k =$

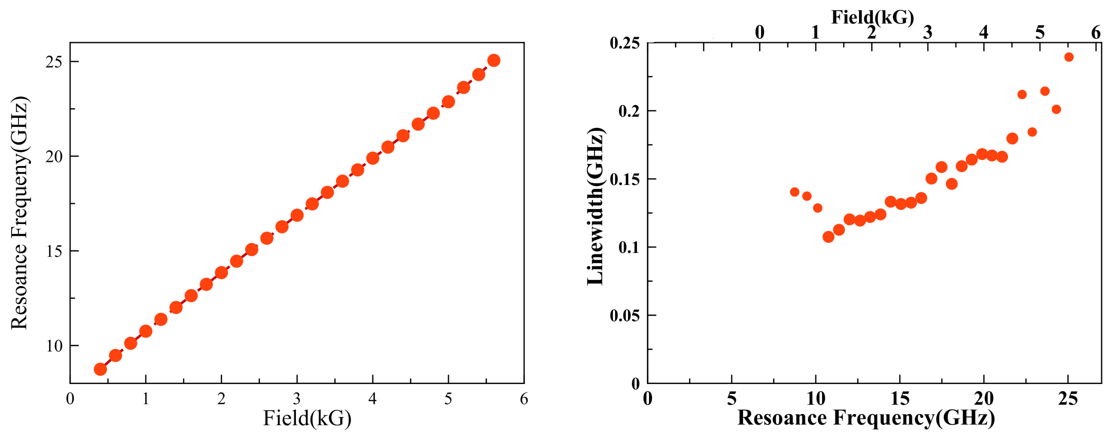


Figure 3.4: (a) Fitted resonance frequency plotted against external magnetic field (b)Fitted linewidth plotted as a function of resonance frequency.

2.5 kG).

Next we try to fit for the damping parameter. Previous work has been shown that Gilbert damping parameter can be determined from the linewidth from the FMR signal[28]. Fig.3.4(b) shows the linewidth plotted as a function of resonance frequency. We would expect to observe a linear relation if only considering Gilbert damping contribution. From our data,however,we can observe obvious two regions which deviate from a simple linear fitting. Firstly, at low frequency around 10GHz, the linewidth was clearly broadened and was larger than other region. Secondly, at higher frequency above 20GHz, the linewidth has more noise in terms of relative fluctuations. Moreover, if we try to fit the linewidth data and extrapolate to zero frequency, we found there is a large non-zero intercept. It is not clear whether this non-zero intercept is due to some inhomogeneous broadening in our sample or some other mechanism. There exist different mechanism responsible for possible linewidth broadening[18].

To fully understand the magnetic dynamics excited in the magnetic tunnel junctions, we make the full ST-FMR measurement and shows the 2D contour plot of the results in Fig.3.5. At lower magnetic field(0 2kG), we can mainly observe three free layer modes. These three modes are parallel to each other and the lowest frequency Q mode is the quasi-uniform mode, which has been used to determine the anisotropy constant. Two higher order mode labeled as

F1 and F2 are distinct from this 2D contour plot although they are hard to distinguish from single spectrum. Starting from 2kG, at lower frequency, there is another mode appearing in the contour plot. This mode,labeled as S mode, has a different dispersion relation: the resonance frequency decreases with increasing magnetic field. This mode can be identified as acoustic mode generating from the SAF layer. The important feature here is that, if we extrapolate the S mode into lower magnetic field, the S mode will be coupled with Q mode around 10GHz at zero field.

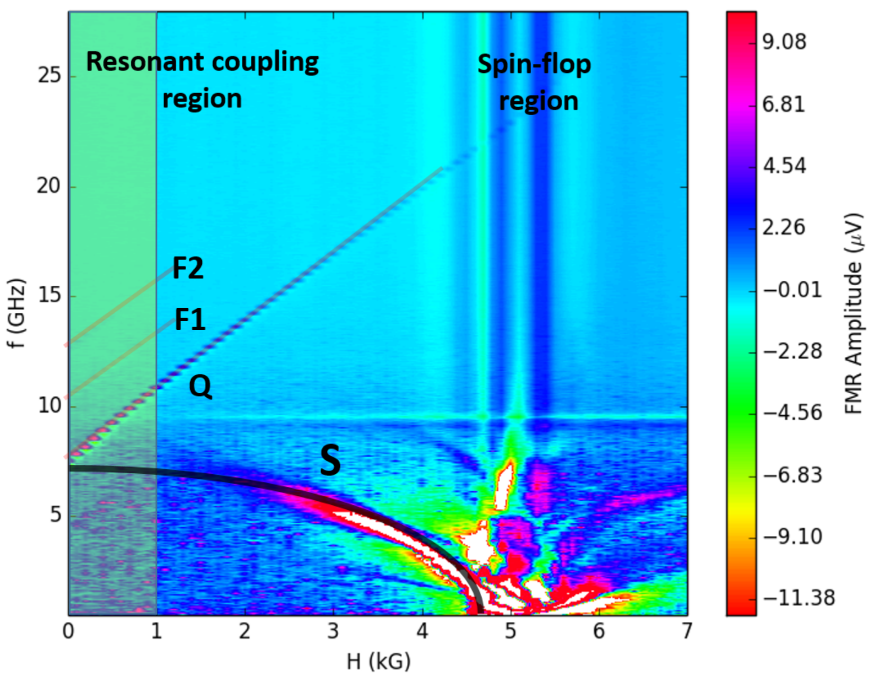


Figure 3.5: ST-FMR spectra measured as a function of out-of-plane magnetic field. Q labels the quasi-uniform mode of the free layer while F2 and F3 are the higher order spin wave modes of the free layer. S labels the acoustic SAF mode.

When we have the resonant coupling between these two modes, the linewidth would be broadened by this resonant coupling mechanism. This is exactly what we have found from Fig.3.5 in the lower frequency region.

In the 2D contour plot, around 4kG magnetic field, as we can see from Fig.3.3(a), the SAF layer becomes unstable and enter the spin-flop region. In this region, because of unstable

SAF layer, the stray field from SAF layer acting on the free layer is also very unstable and produce large magnetic noise during the ST-FMR measurement. As a result, we find there are more fluctuations in the linewidth data as we see from Fig.3.5 around 20GHz.

As we have learned from the 2D contour plot, in order to reliably fit for the damping parameter in the free layer, we need to first exclude the resonant coupling region in the lower frequency, in which the linewidth was broadened by the interaction between free and SAF layer. We also need to avoid the high frequency region. In Fig.3.6 we only include the linewidth data from 10GHz to 20GHz and determine the Gilbert damping to be 0.007 from the slope.

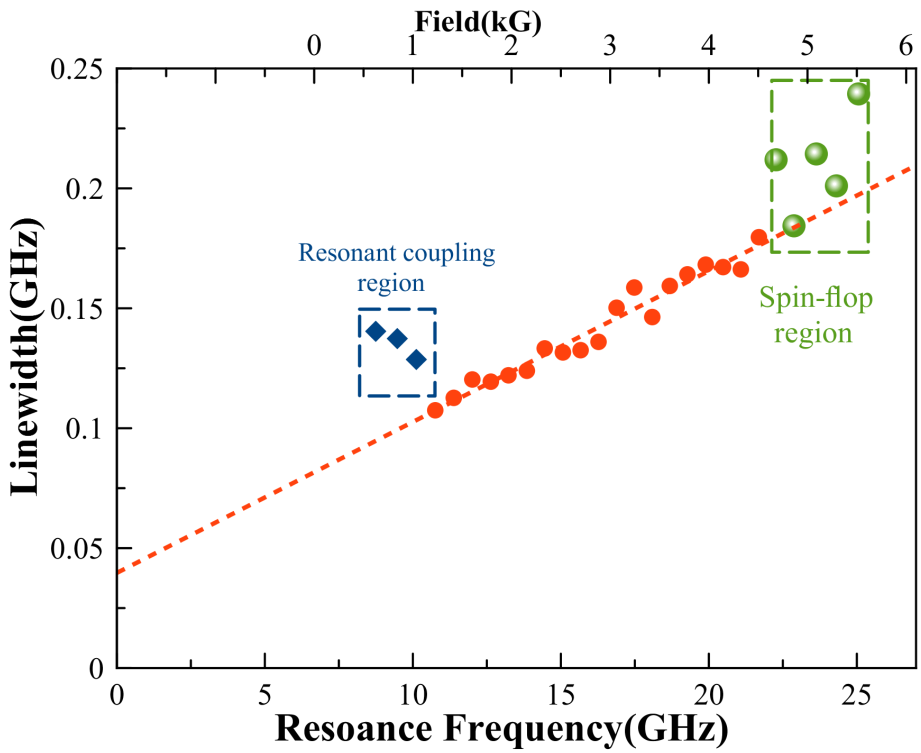


Figure 3.6: Spectral linewidth of the free layer quasi-uniform mode versus frequency of the mode. Line is the best fit to the data outside of the SAF spin flop and SAF resonant coupling regions.

## 3.4 Micromagnetic Simulations

In order to fully understand the magnetic dynamics being excited in the Magnetic Tunnel Junctions, we perform micromagnetic simulations using OOMMF package[4]. To fully account for all magnetic interactions in the MTJ, we use a three dimensional model with three main functional layers: free layer, SAF top and SAF bottom layer. In the simulation, spin wave dynamics is excited by a combined pulse of ST and Oersted field, both resulting from a sinc-shaped spatially uniform current pulse with the amplitude $J_C\frac{\sin(2\pi f_c t^{'})}{2\pi f_c t^{'}}$ with the amplitude the cut-off frequency around 20 GHz, and the time variable $t_0$ 500 ps. The need to combine the excitation from Spin torque and Oersted field is to include the uniform and non-uniform spin wave modes in the MTJs[14]. The spatial profile of the Oersted field is assumed to be that of a long wire with elliptical cross section. The direction of the ST vector acting on the free layer is determined by the magnetization orientation of the SAF top layer.Spectrum of spin wave eigenmodes is obtained via the Fast-Fourier-transform (FFT) of the time dependent in-plane component of the MTJ net magnetic moment.

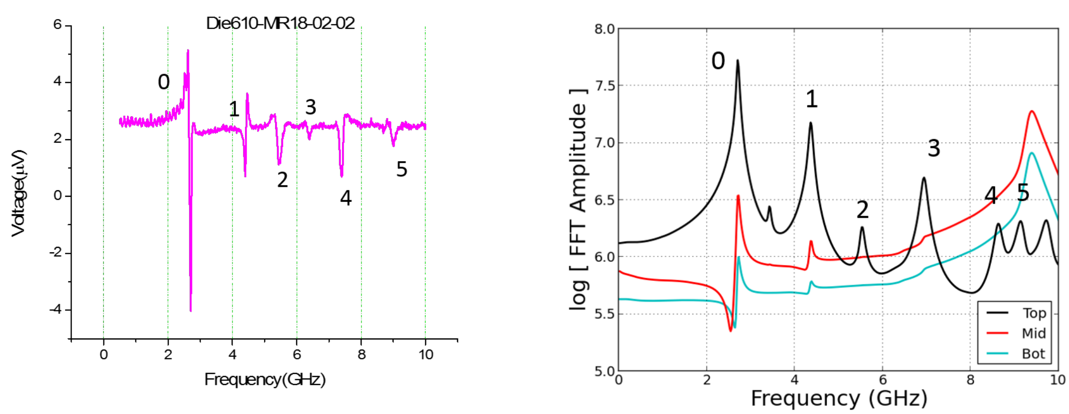


Figure 3.7: (a) ST-FMR spectrum of a 30 nm by 150 nm stadium-shaped STT-MRAM element. Several spin wave eignemode resonances are seen in the spectrum. (b)Fitted spectrum from micromagnetic simluations.

Fig.3.7(a) shows a typical ST-FMR spectrum from our measurement. For this sample, we can identify five spin wave modes. The zero mode is the uniform excitation and we have already used this mode to fit for magnetic anisotropy and Gilbert damping value. The other four modes are non-uniform modes excited along the edges. On the left, Fig.3.7(b) shows the simulated spectrum from our micromagnetic calculations. As we discussed before, we perform the Fast-Fourier-transform on the in-plane component of the MTJ net magnetic moment and plot it against driven frequency. The top layer is the free layer and the middle(bottom) is the SAFTop(SAFBottom) layer. As we can see from the plot, the amplitude of the top layer is definitely much larger than the other layers, meaning the excitation of the MTJs is dominant by the free layer. The peaks in the spectrum are corresponding to the spin wave modes we observe from the experiment. By tuning the material parameter such as magnetic anisotropy and exchange constant, we can match the frequency position of the first zero mode and the second mode. So firstly, from micromagnetic simulations, we can determine the magnetic anisotropy to be $3.13 * 10^5 J/m^3$ and exchange stiffness constant to be around $5 * 10^{-12} J/m$.

Next we would like to understand the nature of the modes we excited. To do this, we perform the spatial mapping of the mode amplitude and plot it in Fig.3.8. Starting from the top left, we list the model profile for all the five modes. As expected, the first mode is uniform excitation so the amplitude of this mode is uniform. The second mode has two nodes along the short axis. So we label it as Mode(2,0). Then we have modes from Mode(3,0) and Mode(4,0) which have three or four nodes along the short axis. The last mode has one node along the long axis, so it is labeled as Mode(0,1).

After that, we find that no matter how we tune the magnetic anisotropy and exchange constant, the latter three modes can not be matched very well from experiment and simulations. So we have to consider another possibilities. One thing to consider is magnetic edge damage of the MTJ element. Such modifications are unavoidable in the STT-MRAM fabrication process due to etching of the element, and they are predicted to have significant impact on current-driven switching of the free layer. We tested several micromagnetic models of the magnetic edge damage and found how these models modify the frequencies of spin wave

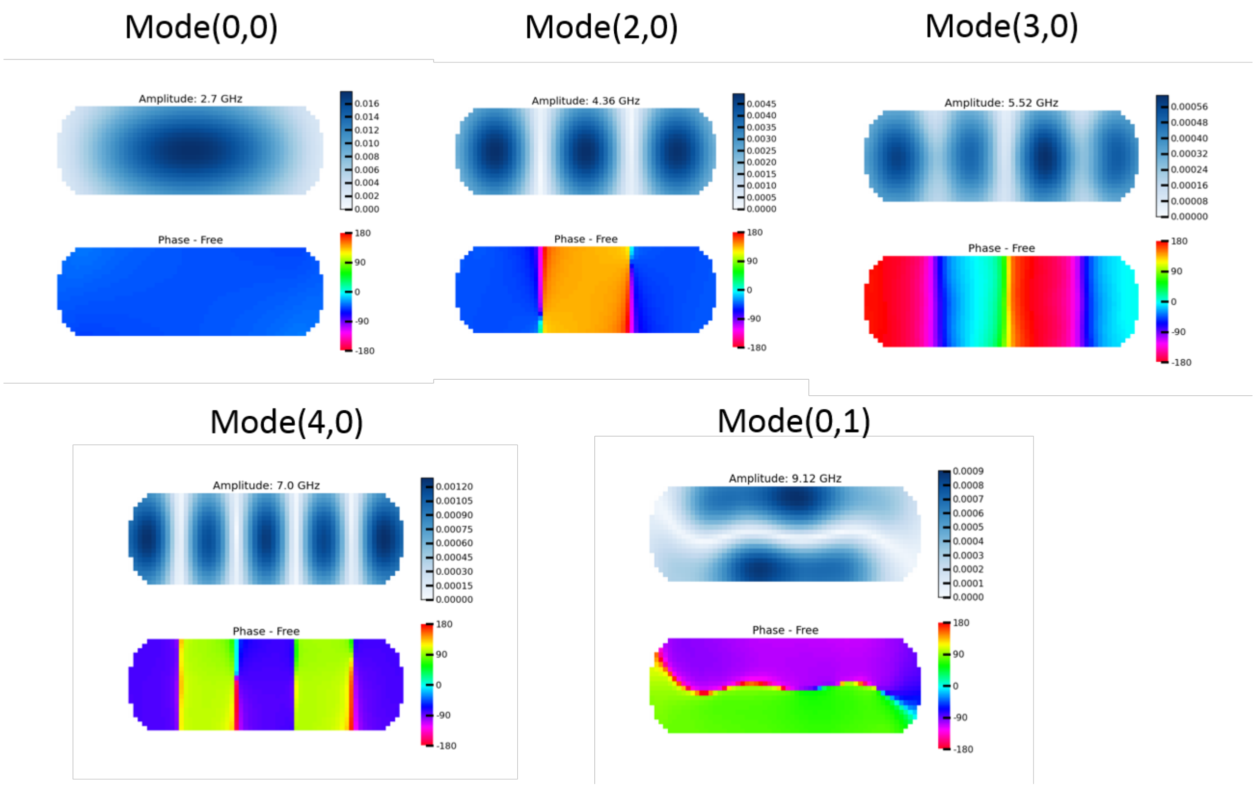


Figure 3.8: Spatial mapping of modes excited in the micromagnetic simulations.

eignemodes. We then compared the models predictions to our measurments of spin wave spectra by spin torque ferromagnetic resonance. This comparison allowed us to determine which model best describes the experimental data. More specifically, we have tested three models of the magnetic edge damage:

- Magnetic dilution model. In this model, saturation magnetization and exchange stiffness of the free layer of STT-MRAM are reduced in the edge region. - STT-MRAM shape distortion model. In this model, the MTJ nanopillar shape is distorted with respect to its nominal shape. - Anisotropy reduction model. In this model, magnetic shape anisotropy is reduced near the sample edges.

Fig.3.9(a) shows the results by exploiting edge damage model in the simulation. From this plot we find that this mode cannot adequately describe the experimentally observed spectrum of spin wave eignemodes in STT-MRAM samples we experimentally studied. Compared with the edge anisotropy model in Fig.3.9(b), now we have a much better agreement between experiment and simulations. We, therefore, conclude that the major impact of the STT-MRAM edge on magnetic properties of the device is reduction of perpendicular magnetic anisotropy near the device edge. This reduction can result in nucleation of current-driven magnetization reversal near the sample edges Comparison of ST-FMR measurements of spin wave mode frequencies can quantify the degree of magnetic anisotropy reduction near the sample edges. We discuss how this can be accomplished in the next paragraph.

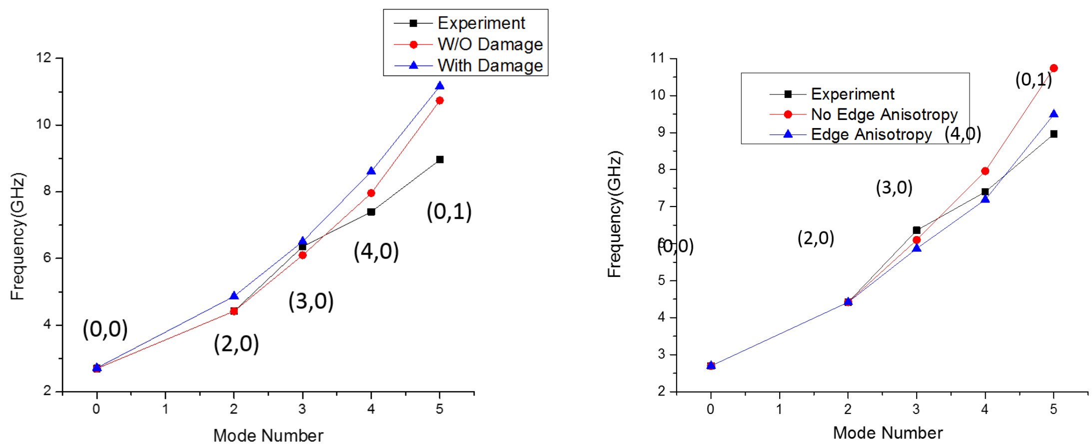


Figure 3.9: (a) ST-FMR spectrum of a 30 nm by 150 nm stadium-shaped STT-MRAM element. Several spin wave eignemode resonances are seen in the spectrum. (b)Fitted spectrum from micromagnetic simluations.

From fitting the first and second mode frequencies, we already have a confidence value of magnetic anisotropy and exchange constant. Then we employ the models of spatially non-uniform parameters of the free layer. The blue symbols in the left panel of Fig.3.9(a) show results of the simulations for the magnetic edge dilution model. In this model, both the saturation magnetization and the exchange constant of the free layer are gradually reduced from their bulk values to zero at the free layer edge. The distance over which this reduction takes place was chosen to be in the 2.5 nm to 7.5 nm range (typical material damage depths due to various types of etching). It is clear from Fig.3.9(a) that the magnetic dilution model does not improve the agreement between theory and experiment. We have also found that shape distortions of the free layer do not reproduce the experimental results well. In contrast, reduction of magnetic anisotropy from $3.13 * 10^5 J/m^3$ in the free layer interior to $3.03 * 10^5 J/m^3$ at the free layer edge over a distance of 2.5 nm gives a much better agreement with the experimental data as shown by blue symbols in the Fig.3.9(b). This type of fitting allows us to obtain the exchange stiffness constant of the free layer, its perpendicular magnetic anisotropy value and the magnitude of reduction of the perpendicular anisotropy at the sample edge.

# Chapter 4

# Time-domain measurement of spin-torque switching in MTJs

As we have discussed in the previous chapter, magnetization switchin induced by spin-tranfer torque is both useful for understanding the fundamental physics of magnetic dynamics and for applications in magnetic random access memory(MRAM). Measurements in the time domain can provide the most direct information about the switching process. However, the majority of previous time-resolved studies of spin-torque switching required averaging over many events, which would hide individual switching variations. Here we report a single-shot time resolved time-domain measurement similar to the technique developed by Cui.et.al [3]. We have shown that the sensitivity of single-shot resistant measurements have been greatly improved and both prior to switching and during spin-torque switching have been resolved.

## 4.1 Experimental Setup

Previously, the sketch of time-domain measurement is shown4.1. The general idea is the following: by send the pulse into the magnetic tunnel junctions, the transmitted the signal will depend on the resistance of the device.

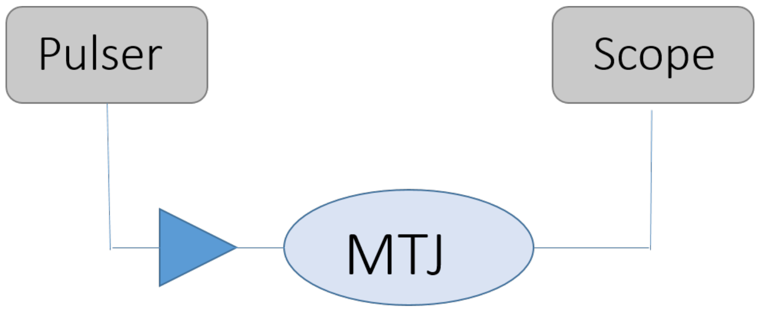


Figure 4.1: Original time-domain setup

If there is magnetic state switching happening during the duration of this pulse, we could be able to resolve it by recording the time-domain signal using a Time scope. This method is very straightforward, however, it is not practical in most cases. To illustrate that, let us calculate the transmitted signal. If we apply the voltage pulse$V_{inc}$, the transmitted signal will be given as

$$V(t) = \frac{V_{inc}}{1 + G_S(t)Z_0/2} \tag{4.1}$$

where $G_S(t) = 1/R_S(T)$ is the sample conductance(the reciprocal resistance), $Z_0 = 50\Omega$ is the probe impedance. Typically the resistance of the devices is around several thousands ohms, so we have a very strong impedance mismatching here. We can expand the time-dependent voltage signal with respect to a reference, if we use the parallel state conductance $G_P$ as the reference value, and write $G_S(t)$ as $G_S(t) = G_P + \Delta G(t)$, since $\Delta G(t)Z_0$ is usually much less than 1, we can expand Equation 4.1 as the following:

$$V(t) = \frac{1}{1 + G_P Z_0/2} V_{inc} + \frac{Z_0/2}{(1 + G_P Z_0/2)^2} V_{inc} \Delta G(t) \tag{4.2}$$

The first term in Equation4.2 is related to the resistance mismatch between the device and RF probe. The second term is coming from the resistance change associated with magnetic dynamics. If we would like to monitor the device resistance, we should expect the second term to be large, at least well above the noise level. However, as we point out, because of the impedance mismatching, the second term would be really smaller, usually around several mill volts. This requires lots of averaging to improve the signal to noise ratio and thereby hide each single switching event.

To improve our signal to noise ratio, we adapt improved measurement set-up shown in Fig.4.2. As usual, we apply the pulse from a pulse generator. This time, however, we split the into two identical copies. The first copy goes into the device and induce magnetic switching. The second pulse will go through a pulse inverter and it will flip the polarity. What is important here is to choose the pulse inverter so that it does not distort the waveform too much. After the first copy goes through the device, we use a power combiner to combine these two pulses in a way that these two copies should enter the power combiner at the same time.

To accomplish that, we would like to carefully tune the time delay of there two lines so that they have been correctly synchronized. In the current set-up, we adjust the time delay by varying the microwave cable length in the circuit. After we combine these two pulses, we use an amplifier to amplify the signal and send it into the storage scope. In this process, the signal left after we combine these two pulses would only be the part depending on the magnetic state, where any other type of noise should be canceled out. This should greatly improve the signal-to-noise ratio.

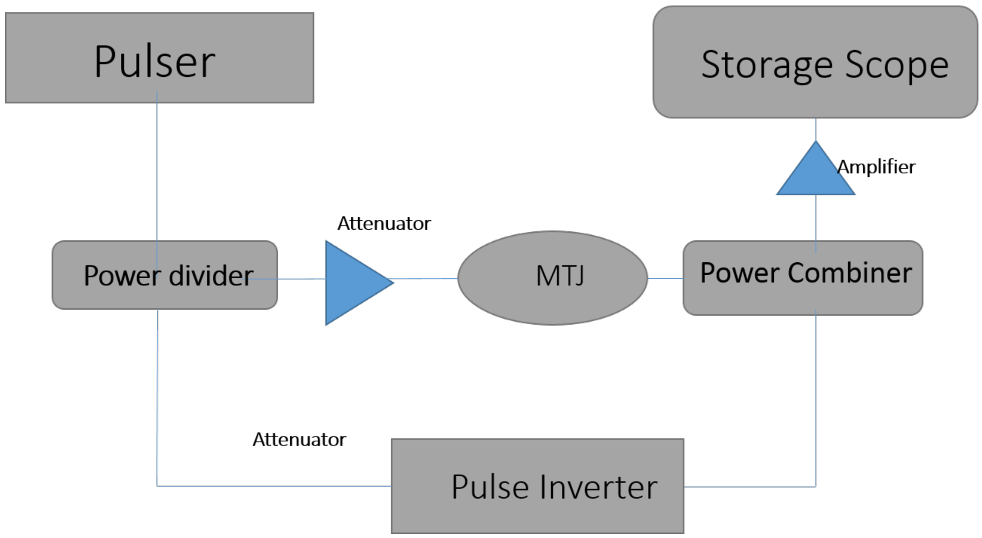

Figure 4.2: Improve time-domain set-up

Before we go to the experiment discussion, we would like to discuss another important source of noises in these type of experiments. Ideally, we want to amplify our voltage signal after the power combiner to be large enough. However, we also have to fight with the bit noise induced by the storage scope. We are using a 64-bit time scope, the bit noise in the measurement is proportional to the voltage resolution used in the time scope. So in order to reduce the bit noise, smaller voltage resolution should be adapted and the signal has to be small enough to fit in this small voltage resolution. Practically, after we amplify the voltage signal, we use proper attenuator(usually around -10 dB).

## 4.2 Results and Discussion

Now we have set-up correct time delay and pick appropriate attenuation in the circuit, we can send the pulse and observe the time dependent signal. Fig.4.3 shows a typical signal we resolve from a switching. We first initialize the MTJ into anti-parallel state and send through a positive pulse. The polarity of positive pulse corresponds to damping for the anti-parallel state, so this positive pulse should not induce magnetic switching for anti-parallel state. We record the anti-parallel state signal as the background and label it as AP in Fig.4.3.

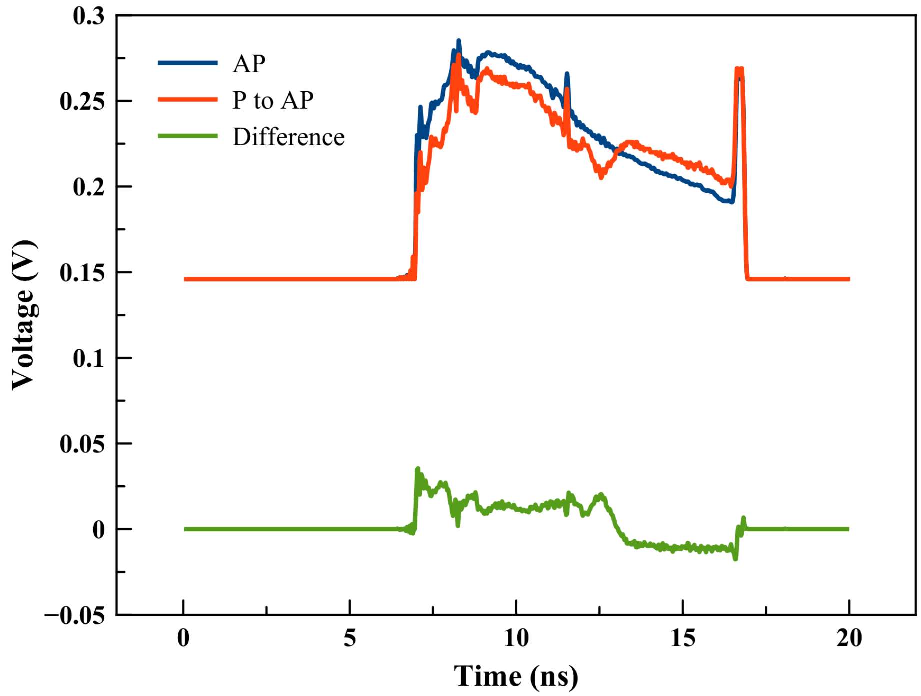


Figure 4.3: A switching signal from time-domain measurement. Anti-parallel signal(blue), PtoAP signal(red) along with the voltage difference(Green)

Then, we initialize the MTJ into parallel state and re-send the positive voltage(which is anti-damping for parallel state). Then we record this signal from the time scope and label as P to AP in Fig.4.4(a). One can clearly find that at the beginning of the pulse, AP and PtoAP signal are clearly separated. At the middle of the pulse, the PtoAP pulse suddenly shifts into AP signal, which is related to the magnetic state change in the MTJ. So we have observe a magnetic switching in time-domain. We can also subtract the background AP signal from the PtoAP and plot it labeled as Difference in Fig.4.4(b). If we look at the Difference signal, we can see that at the beginning of the pulse, the difference is around 30 mV, then it drops to - 10 mV. So we can well separate the anti-parallel and parallel state.

Now that we have greatly improved the voltage signal to separate two magnetic states, we can study individual switching event without perform averaging to reduce the noise. One

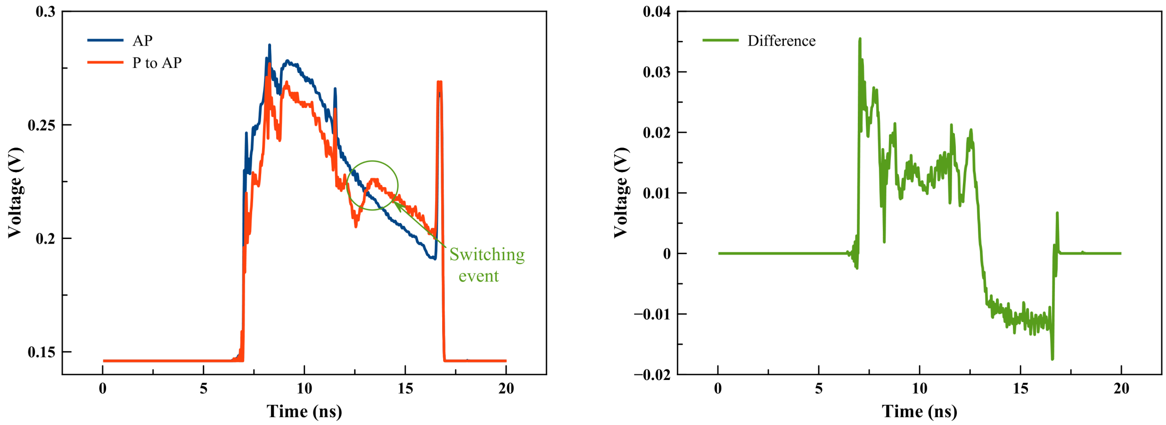


Figure 4.4: (a) Zoomed PtoAP signal(red) and AP state background(blue) (b)Zoomed voltage signal difference.

thing we can study is the distribution of switching time. From Fig.4.5(a) to Fig.4.5(c) we show several traces from different switching events. Here we only demonstrate the different signals between two state. One can clear find that for different switching traces, we have different switching time, ranging from 2.6 ns, which is at the beginning of the pulse, to 9 ns, which is at the very end of the pulse. This indicates the random nature of this single shot-switching. More importantly, we can obtain a good statistics of switching time as a function of input parameters. Also we find that in Fig.4.5(d) we find that at a fixed voltage, we can still have non-successful switching event, where we find that for this non-successful switching attempt, the system enters a large oscillation. This enables us to further study the different between successful and non-successful switching events.

To further illustrate the random nature of magnetic switching in time-domain, we fix the applied voltage at 425 mV and study the distribution of the switching time as it is shown in Fig.4.6. From other switching probability measurement, we already know that at 425 mV voltage, the device has a very switching probability. From this distribution we find that the switching time is unevenly distributed, it is centered around 4 ns and has a negative skewness. The distribution also gives a very small tail at high switching time, which means switching rarely happens at the tail of the pulse. We try to fit the switching count as a

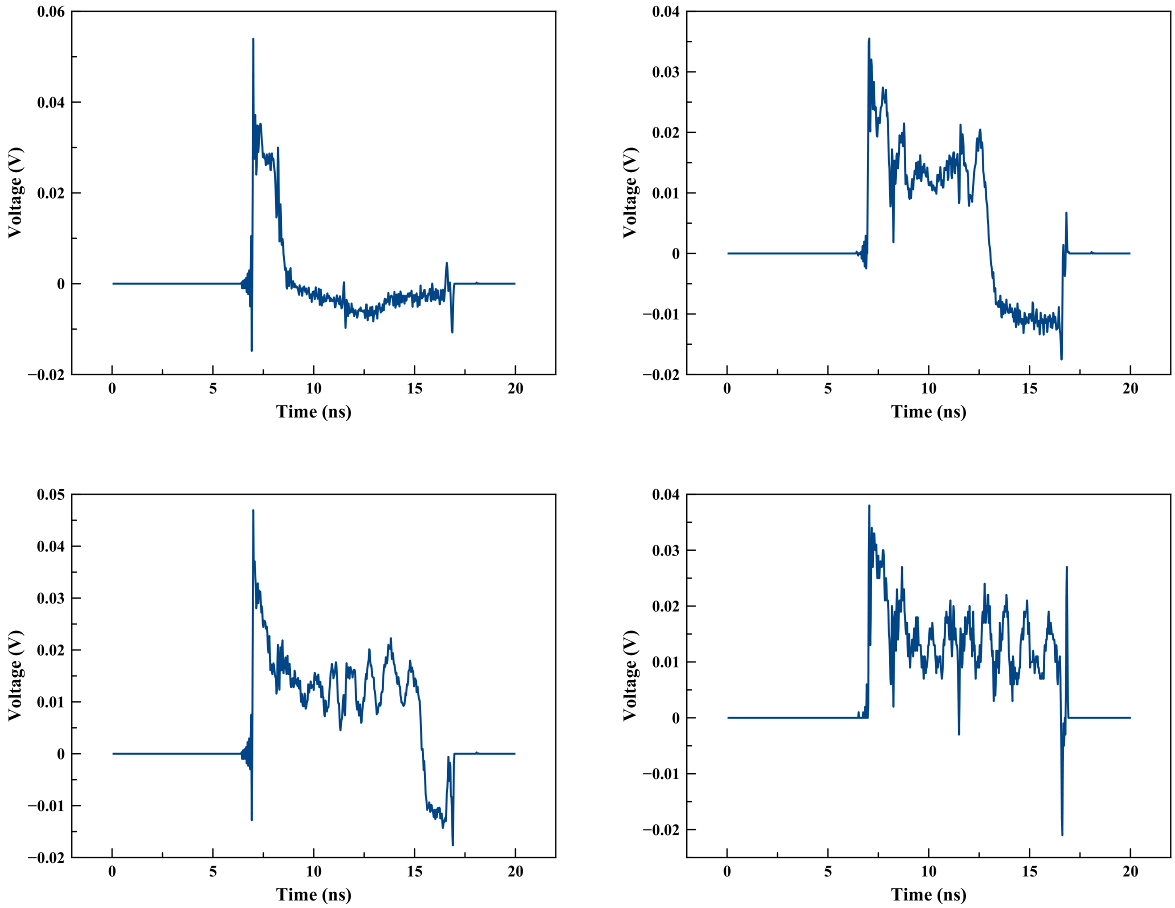


Figure 4.5: Switching events for different individual events.(a)(b)(c) show switching events which switch at 2.6 ns, 6.7 ns and 9 ns respectively. (d) shows the non-switching event.

Gaussian function, which gives a good fitting result as it is shown in Fig.4.6.

If we vary the applied voltage and also measure the switching time distribution as Fig.4.6, we typically find that the the peak of the distribution and also the skewness are dependent on the applied voltage. For smaller applied voltage, the center of the switching time moves to higher time period and the skewness of the distribution becomes smaller. That indicates that for larger voltage we have more deterministic and fast switching. When the applied voltage is small and the switching probability is low, the switching behavior shows more randomness.

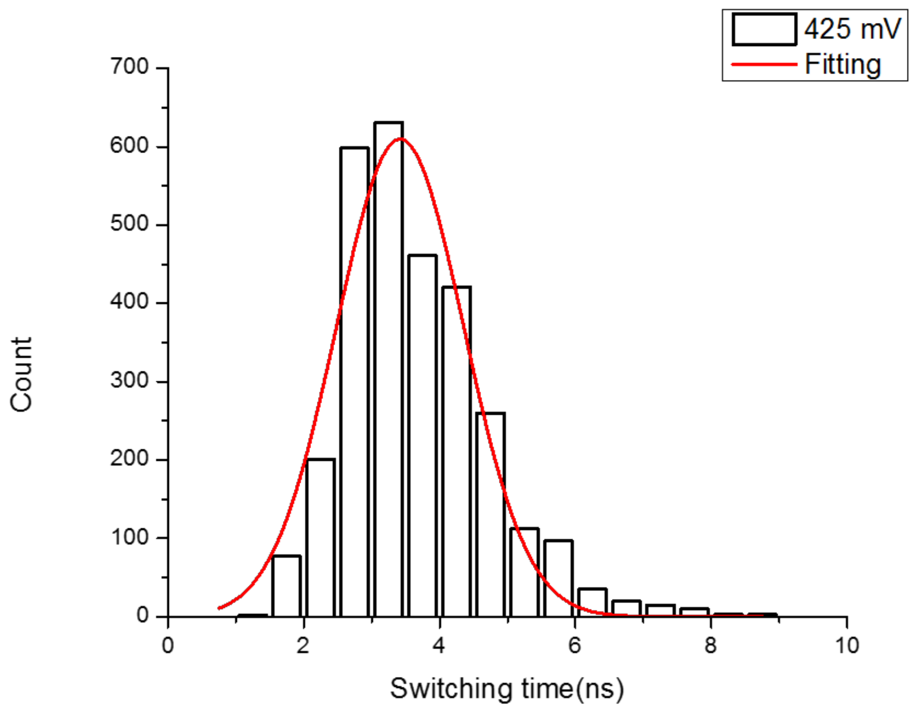


Figure 4.6: Distribution of switching time at constant voltage 425 mV.

# Chapter 5

# Write Error Rate measurement

In order to make magnetic tunnel junctions as the cell for future Magnetic Random Access memory, it is important to characterize the switching property for MTJs, which setting the MTJs to a desired state(write). This measurement is known as the Write Error Rate(WER). Formally, applying the electric pulse at different duration and amplitude, by monitoring the resistance before and after the pulse, we can find the switching probability. For optimizing the WER, we need to consider the power consumption and also the switching time. Moreover, from a fundamental physical point of view, it is important to understand the detailed switching mechanism. In the previous chapter, we have already shown how to observe switching in time-domain.

The Write Error Rate(WER) is defined as the ratio between number of non-switching attempt with the total switching attempt. So WER can be understood as the probability of not successful attempt. The typical error used in common computer memory is around $10^{-9}$. Therefore, in order to reliably characterize the WER, we need to obtain very large statistics, which is only increasing by taking into account the approximately $\sqrt{N}$ counting error associated with the binary results of a switching attempt. It would take years by employing conventional DC resistance measurement in this sense. To overcome this, we are going to a quick and accurate measurement of WER with large statistics as a function of certain parameters.

## 5.1 Experimental Setup

We first show the experiment set-up for write error rate measurement5.1. As we can see, the circuit has been divided into two parts. In the AC part, a Picosecond Pulse Labs 10,0070A pulse generator (PSPL) is used to generate write pulses and an Agilent 33220A Arbitrary Waveform Generator (ARB) provides the reset pulse. We then use a Keithley 2400 source Meter(Keithley) to provide a small DC bias voltage, which will then be National Instruments USB-6251 BNC Digital Acquisition Board (DAQ)

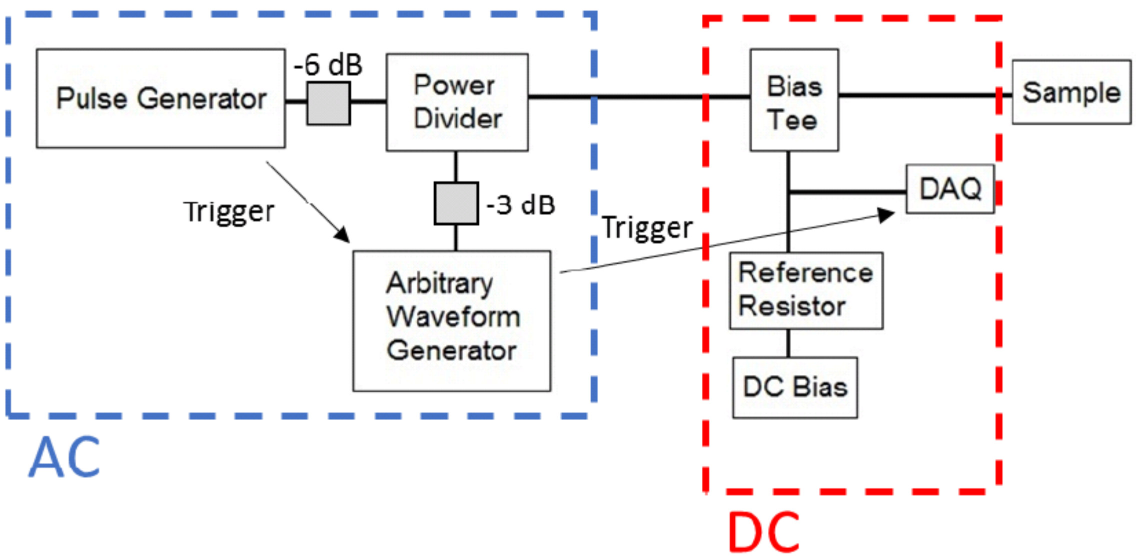


Figure 5.1: Write Error Rate measurement set-up, here we include AC and DC circuit

The PSPL can provide pulses from 100 picosends to 10 nanoseconds, while the ARB has a pulse range from 50 nanoseconds to DC. Our goal is to generate a pulse sequence as it is shown in 5.2.

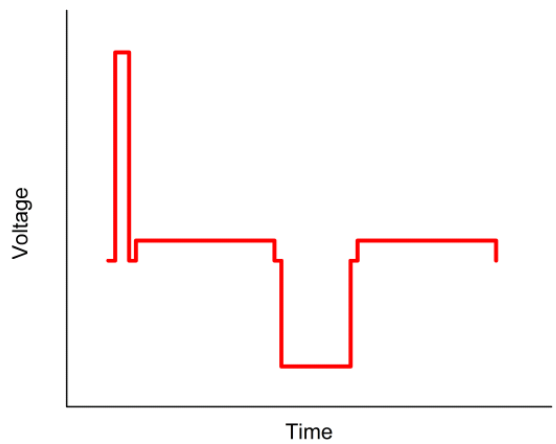


Figure 5.2: Pulse shape used in Write Error Rate Measurement

In order to produce such a pulse sequence, we need to establish correct synchronization. To do that, the following procedure has been carried out:

1. Connect the trigger output of the PSPL to the trigger input of the ARB. This port of the ARB is labeled Ext. Trig., which is located on the rear panel.

2. Set the PSPL trigger method to Internal with a repetition rate appropriate for the length of pulse train used (for the work presented in this thesis, 2.5 kHz was used). Now the PSPL is used to control the remaining instruments

3. Set the ARB trigger to Ext. Trig. (rising edge) and the output mode to Burst. This will allow the ARB to generate a bust of pulse sequence once tiggered.

4. Connect the trigger output of the ARB (labeled Sync) to the trigger input of the DAQ, labeled APFI0 (analog programmable function interface) for the model mentioned above.

5. Set the DAQ trigger to APFI0 and the sampling rate to maximum (1.25 MSamples/s in the case of this DAQ)

6. Connect a reference resistor to the DC bias and then connect it to the DC port of the bias tee. Usually this reference resistor should have resistance in the middle of parallel and

anti-parallel state. The DC bias should have constant output and is chosen to have a polarity to favor the switched state.

7. Connect an analog input of the DAQ (any will do) between the reference resistor and the bias tee.

8. Connect the outputs of the PSPL and ARB, with appropriate attenuators to protect the equipment at the hardware level (for the equipment and circuit used here, -6 dB and -3 dB respectively), to the power divider. Then connect the remaining port of the power divider to the AC port of the bias tee. All connection cables used should be rated for the appropriate frequency of the pulses.

The logical behind the experiment setup is explained the following. To measure the switching probability at a fixed pulse, we need to record the resistance before the pulse and after the pulse. Clearly, it would not be practicable to measure the resistance using a Keithley(it would be painfully slow). By inserting a reference resistor between the sample and DC source, the voltage passing through the reference resistor would change according to the sample resistance. By recording the voltage in real time, we can record the resistance of the sample.

Another import aspect of the measurement is to properly reset the state. Of course, using a magnetic field to reset is not acceptable. To accomplish that, we use ARB to generate a opposite pulse as write pulse. To save the sample from electrical breakdown, the reset pulse is usually longer than write pulse and should have relatively low amplitude.

The raw data we get from the automation software such as LabView would be a voltage trace of many switching attempts. Usually LabView is not efficient enough to handle such a great amount of data. So we choose to have LabView to extract two sections of each switch attempt corresponding to the read pulse and write pulse. This method will give us a long list of initial and final voltages from each switching attempt that can be then translate into resistance and then compare to evaluate the success of each switching attempt.

Given the voltage recorded by the DAQ, we can convert the voltage to resistance of the sample. The DC part of the circuit is a voltage divider, the resistance of the MTJ as a function of the measured DAQ voltage $V_{\mathrm{DAQ}}$ is given by

$$R_{\mathrm{MTJ}} = \frac{R_{\mathrm{Ref}} V_{\mathrm{DAQ}}}{V_{\mathrm{DAQ}} - V_{\mathrm{Read}}} \tag{5.1}$$

where$R_{\mathrm{Ref}}$ is the value of the reference resistor and $V_{\mathrm{Read}}$ is the read voltage. Here the value of $V_{\mathrm{Read}}$ should be properly picked. The read voltage should be higher enough to well separate two states, at the same time, higher read voltage would disturb the switching state. To show that, the voltage difference between anti-parallel state and parallel state is the following:

$$\Delta V_{\mathrm{DAQ}} = V_{\mathrm{read}} \frac{(R_{\mathrm{AP}} R_{\mathrm{Ref}} - R_{\mathrm{P}} R_{\mathrm{Ref}})}{(R_{\mathrm{AP}} + R_{\mathrm{Ref}})(R_{\mathrm{P}} - R_{\mathrm{Ref}})} \tag{5.2}$$

where $R_{\mathrm{AP}}$ and $R_{\mathrm{P}}$ are anti-parallel and parallel resistance of the device. Here we find that the voltage difference is linearly depend on the read voltage.

Now we have to determine an adequate and safe reset voltage and process the raw data output by LabView. One first needs to process some initial data and then optimize based upon the results in an iterative fashion to assess the efficiency of the reset pulse. To analyze the raw data file, a python script carry out the following routine:

1. Read the raw data file and extract all initial and final measured voltage(before and after pulse.)

2. Convert the raw voltage into resistace using Equation5.2.

3. Determine the device state for each voltage value. This can be done by considering the known parallel and anti-parallel states. Usually, if the read voltage is positive, the AP state should have higher voltage.

4. Compare initial and final voltage for each switching attempe and categorize into three possible cases: switched(the device starts in the correct state and ended in the opposite state), not-switched(the device starts in the correct state and fail to switch), and missed(the device starts at the wrong state.)

5. Sum over all the switching attempt. The write error rate is given as $\frac{N_{NotSwitched}}{N_{attempts}-N_{missed}}$

To determine the necessary reset voltage, we adapt the following iterative process:

1. Set the write voltage so that most of the switching attempts are successful.

2. Set the reset voltage to a safe and small amount. A good starting point is half of the write voltage.

3. Start the measurement and process the data. Identify the number of missed events, which means the device has not been set properly to the desired initial state.

4. Slowing increase the reset voltage so that the number of missed event is much less than one per cent of the total switching events.

Since the duration of the reset pulses are much longer than write pulses(typical resets pulse duration are 100 500 ns while write pulses are usually smaller than 10 ns). The proper value of reset pulse is very important for this measurement. If the reset pulse is too small, then many of switching attempts would not be used in the final data analysis. If the reset pulse is too large, then we take the risk of device breakdown. Now with our measurement technique explained, we can reliably and efficiently study Write Error Rate as a function of write pulse and voltage, applied magnetic field or any other interesting parameters. With our experimental set-up, $10^6$ switching attempts can be completed in 8.5 minutes.

## 5.2 Results and Discussion

Detailed switching mechanism by applying the spin transfer torque is still unclear. People have argued that it is possible some sub-area will act as an activation regime which will leads the switching[25]. It is proposed that at finite temperature, switching probability is proportional to applied voltage[23]. However recently people have found anomalous behavior at certain amplitude and polarity[15][24][31]. We would like to test the switching probability measurement on our samples.

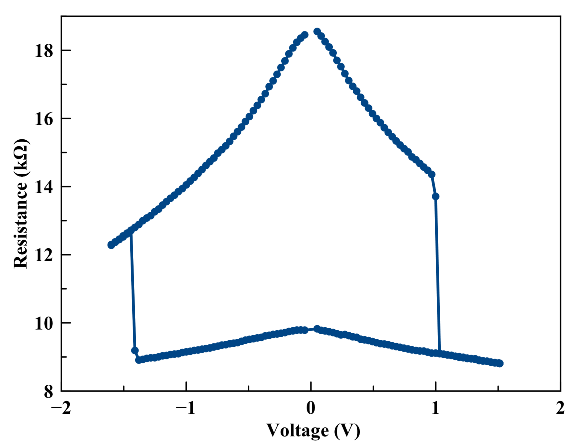


Figure 5.3: Resistance versus dc voltage at zero magnetic field

Before we make Write Error Rate measurement, we need to measure the resistance as a function of dc voltage to identify the switching probablity. Fig.5.3 shows one example of sample resistance as a function of applied dc voltage. At positive polarity, the device starts at high-resistance(anti-parallel)state. The resistance drops with increasing voltage. Around 1 V, the resistance drops to low-resistance(parallel)state and stay at parallel state when the voltage keep increasing. Now if we keep the device to be in the parallel state and start to apply the negative voltage, around negative 1.5 V, the resistance of the device will go up, which means switching from parallel to anti-parallel. So from this curver we know that by applying the postive voltage pulse, we can switch the device from anti-parallel state to parallel state.

To perform the write error rate measurement, we first initialize the device at the anti-parallel state using magnetic field, then we constantly apply the positive voltage as we dicussed in the previous section. Appropriate reset voltage has been chosen to reset the device back into anti-parallel state. In this set-up of measurement we fix the pulse duration to be 10 ns and only varying the pulse amplitude. The result is shown in Fig.5.4

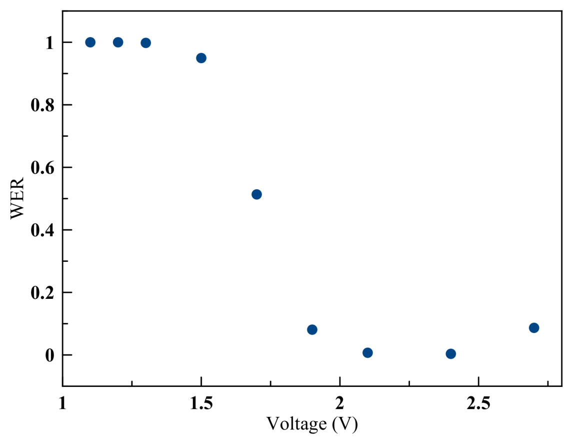


Figure 5.4: Write Error Rate curve for one typical device studied in the experiment.

At low amplitude pulse, the switching probability is indeed very low, close to zero. As we gradually increase the pulse amplitude, around 1.5 V, the device start to increase and the WER is close to zero at around 2 V applied voltage. So far everything is as expected. However, starting from 2 V when we would normally expect the WER to keep decreasing at increasing applied voltages, we find that however, the WER start to increase somehow. More formally, from a uniform switching theory, the WER should have Gaussian dependence with respect to voltage at finite temperature[15], so we can call this non-Gaussian behavior to be anomalous WER.

Different mechanism has been proposed to explain the anomalous WER behavior. One possible origin is coming from non-linear coupling between modes excited in MTJs [5][29]. Another suspect is the formation of sub-volume domain in the switching process. Previously, people believe that the switching process is dominate by sub-volume switching[9][25]. However now there is a growing evidence to show that the Dzyaloshinskii-Moriya interaction can significantly affect the switching process and cause the meta-stable state which is unfavorable for switching[20].

# Chapter 6

# Conclusion

In chapter 3, we demonstrate that by employing field modulation technique in spin-torque ferromagnetic resonance measurement, we can greatly improve the signal-to-noise ratio and are able to accurately determine important material parameters such as magnetic anisotropy, Gilbert damping in nanoscale magnetic tunnel junctions. This result is essential in understanding magnetic dynamics driven by spin transfer torque in nanomagnets. In chapter 4, we focus on time-domain measurement of spin transfer torque driven switching. With great improvement in the measurement sensitivity, now we are able to resolve single shot switching signal without performing averaging which will hide individual variations. By studying the statistics of the switching time, we can observe voltage-dependent behavior during the magnetic switching. In chapter 5, we focus on measurement of switching probability of magnetic tunnel junctions by applying electric pulses. We observe anomalous write error rate behavior in our magnetic tunnel junctions samples. Possible origins of this anomalous write error rate has been discussed.

In the future, we would like to study the correlations between these characterization technique. Once we identify magnetic tunnel junction samples showing anomalous write error rate, we can perform spin-torque ferromagnetic resonance measurement with field modulation to study the spin wave spectrum and non-linear coupling between spin wave modes. Single-shot time-domain measurements on samples showing anomalous samples will show sight into difference between successful switching events between unsuccessful switching events. This will allow us to understand deeply about spin-torque driven magnetic dynamics in nanomagnets.

# Bibliography

[1] A. Brataas, A. D. Kent, and H. Ohno. Current-induced torques in magnetic materials. *Nat Mater*, 11(5):372–381, May 2012.

[2] W. H. Butler, X.-G. Zhang, T. C. Schulthess, and J. M. MacLaren. Spin-dependent tunneling conductance of Fe|MgO|Fe sandwiches. *Phys. Rev. B*, 63:054416, Jan 2001.

[3] Y.-T. Cui, G. Finocchio, C. Wang, J. A. Katine, R. A. Buhrman, and D. C. Ralph. Single-shot time-domain studies of spin-torque-driven switching in magnetic tunnel junctions. *Phys. Rev. Lett.*, 104:097201, Mar 2010.

[4] M. J. Donahue and D. G. Porter. OOMMF User's Guide, Version 1.0, 1999.

[5] E. R. Evarts, R. Heindl, W. H. Rippard, and M. R. Pufall. Correlation of anomalous write error rates and ferromagnetic resonance spectrum in spin-transfer-torque-magnetic-random-access-memory devices containing in-plane free layers. *Applied Physics Letters*, 104(21), 2014.

[6] G. D. Fuchs, J. C. Sankey, V. S. Pribiag, L. Qian, P. M. Braganca, A. G. F. Garcia, E. M. Ryan, Z.-P. Li, O. Ozatay, D. C. Ralph, and R. A. Buhrman. Spin-torque ferromagnetic resonance measurements of damping in nanomagnets. *Applied Physics Letters*, 91(6), 2007.

[7] A. M. Gonalves, I. Barsukov, Y.-J. Chen, L. Yang, J. A. Katine, and I. N. Krivorotov. Spin torque ferromagnetic resonance with magnetic field modulation. *Applied Physics Letters*, 103(17), 2013.

[8] A. Helmer, S. Cornelissen, T. Devolder, J.-V. Kim, W. van Roy, L. Lagae, and C. Chappert. Quantized spin-wave modes in magnetic tunnel junction nanopillars. *Phys. Rev. B*, 81:094416, Mar 2010.

[9] Y. Huai, F. Albert, P. Nguyen, M. Pakala, and T. Valet. Observation of spin-transfer switching in deep submicron-sized and low-resistance magnetic tunnel junctions. *Applied Physics Letters*, 84(16):3118–3120, 2004.

[10] M. Julliere. Tunneling between ferromagnetic films. *Physics Letters A*, 54(3):225 – 226, 1975.

[11] C. Kittel. On the theory of ferromagnetic resonance absorption. *Phys. Rev.*, 73:155–161, Jan 1948.

[12] X. Liu, W. Zhang, M. J. Carter, and G. Xiao. Ferromagnetic resonance and damping properties of cofeb thin films as free layers in mgo-based magnetic tunnel junctions. *Journal of Applied Physics*, 110(3), 2011.

[13] MaruyamaT., ShiotaY., NozakiT., OhtaK., TodaN., MizuguchiM., T. A., ShinjoT., ShiraishiM., MizukamiS., AndoY., and SuzukiY. Large voltage-induced magnetic anisotropy change in a few atomic layers of iron. *Nat Nano*, 4(3):158–161, Mar 2009.

[14] R. D. McMichael and M. D. Stiles. Magnetic normal modes of nanoelements. *Journal of Applied Physics*, 97(10), 2005.

[15] T. Min, J. Z. Sun, R. Beach, D. Tang, and P. Wang. Back-hopping after spin torque transfer induced magnetization switching in magnetic tunneling junction cells. *Journal of Applied Physics*, 105(7), 2009.

[16] V. V. Naletov, G. de Loubens, G. Albuquerque, S. Borlenghi, V. Cros, G. Faini, J. Grollier, H. Hurdequint, N. Locatelli, B. Pigeau, A. N. Slavin, V. S. Tiberkevich, C. Ulysse, T. Valet, and O. Klein. Identification and selection rules of the spin-wave eigenmodes in a normally magnetized nanopillar. *Phys. Rev. B*, 84:224423, Dec 2011.

[17] H. T. Nembach, J. M. Shaw, C. T. Boone, and T. J. Silva. Mode- and size-dependent landau-lifshitz damping in magnetic nanostructures: Evidence for nonlocal damping. *Phys. Rev. Lett.*, 110:117201, Mar 2013.

[18] C. L. Ordóñez Romero, B. A. Kalinikos, P. Krivosik, W. Tong, P. Kabos, and C. E. Patton. Three-magnon splitting and confluence processes for spin-wave excitations in yttrium iron garnet films: Wave vector selective brillouin light scattering measurements and analysis. *Phys. Rev. B*, 79:144428, Apr 2009.

[19] D. Ralph and M. Stiles. Spin transfer torques. *Journal of Magnetism and Magnetic Materials*, 320(7):1190 – 1216, 2008.

[20] J. Sampaio, A. V. Khvalkovskiy, M. Kuteifan, M. Cubukcu, D. Apalkov, V. Lomakin, V. Cros, and N. Reyren. Disruptive effect of dzyaloshinskii-moriya interaction on the magnetic memory cell performance. *Applied Physics Letters*, 108(11), 2016.

[21] J. C. Sankey, P. M. Braganca, A. G. F. Garcia, I. N. Krivorotov, R. A. Buhrman, and D. C. Ralph. Spin-transfer-driven ferromagnetic resonance of individual nanomagnets. *Phys. Rev. Lett.*, 96:227601, Jun 2006.

[22] Y.-T. S. J. C. B. R. A. R. D. C. Sankey, Jack C. Cui. Measurement of the spin-transfer-torque vector in magnetic tunnel junctions. *Nat Phys*, 4(1):67–71, Jan 2008.

[23] J. Sun. Current-driven magnetic switching in manganite trilayer junctions. *Journal of Magnetism and Magnetic Materials*, 202(1):157 – 162, 1999.

[24] J. Z. Sun, M. C. Gaidis, G. Hu, E. J. OSullivan, S. L. Brown, J. J. Nowak, P. L. Trouilloud, and D. C. Worledge. High-bias backhopping in nanosecond time-domain spin-torque switches of mgo-based magnetic tunnel junctions. *Journal of Applied Physics*, 105(7), 2009.

[25] J. Z. Sun, R. P. Robertazzi, J. Nowak, P. L. Trouilloud, G. Hu, D. W. Abraham, M. C. Gaidis, S. L. Brown, E. J. O'Sullivan, W. J. Gallagher, and D. C. Worledge. Effect of subvolume excitation and spin-torque efficiency on magnetic switching. *Phys. Rev. B*, 84:064413, Aug 2011.

[26] A. A. Tulapurkar, Y. Suzuki, A. Fukushima, H. Kubota, H. Maehara, K. Tsunekawa, D. D. Djayaprawira, N. Watanabe, and S. Yuasa. Spin-torque diode effect in magnetic tunnel junctions. *Nature*, 438(7066):339–342, Nov 2005.

[27] C. Wang, Y.-T. Cui, J. A. Katine, R. A. Buhrman, and D. C. Ralph. Time-resolved measurement of spin-transfer-driven ferromagnetic resonance and spin torque in magnetic tunnel junctions. *Nat Phys*, 7(6):496–501, Jun 2011.

[28] C. Wang, Y.-T. Cui, J. Z. Sun, J. A. Katine, R. A. Buhrman, and D. C. Ralph. Bias and angular dependence of spin-transfer torque in magnetic tunnel junctions. *Phys. Rev. B*, 79:224416, Jun 2009.

[29] C. Wang, H. Seinige, and M. Tsoi. Current-driven parametric resonance in magnetic multilayers. *Journal of Physics D: Applied Physics*, 46(28):285001, 2013.

[30] W.-G. Wang, M. Li, S. Hageman, and C. L. Chien. Electric-field-assisted switching in magnetic tunnel junctions. *Nat Mater*, 11(1):64–68, Jan 2012.

[31] Z. Wang, Y. Zhou, J. Zhang, and Y. Huai. Bit error rate investigation of spin-transfer-switched magnetic tunnel junctions. *Applied Physics Letters*, 101(14), 2012.

[32] L. Xue, C. Wang, Y.-T. Cui, J. A. Katine, R. A. Buhrman, and D. C. Ralph. Network analyzer measurements of spin transfer torques in magnetic tunnel junctions. *Applied Physics Letters*, 101(2), 2012.

[33] J. Zhu, J. A. Katine, G. E. Rowlands, Y.-J. Chen, Z. Duan, J. G. Alzate, P. Upadhyaya, J. Langer, P. K. Amiri, K. L. Wang, and I. N. Krivorotov. Voltage-induced ferromagnetic resonance in magnetic tunnel junctions. *Phys. Rev. Lett.*, 108:197203, May 2012.